Hindawi
Journal of Nanomaterials
Volume 2019, Article ID 2710712, 8 pages
https://doi.org/10.1155/2019/2710712

Research Article

CoS/Nanocarbon Composite as a Catalytic Counter Electrode for Improved Performance of Quantum Dot-Sensitized Solar Cells

Wen Yang,[1] Yang Sun,[2] Peizhi Yang ,[1] and Xiaobo Chen [2]

[1]*Key Laboratory of Education Ministry for Advance Technique and Preparation of Renewable Energy Materials, Yunnan Normal University, Kunming 650500, China*
[2]*School of New Energy and Electronic Engineering, Yancheng Teachers University, Yancheng 224051, China*

Correspondence should be addressed to Peizhi Yang; pzhyang@hotmail.com and Xiaobo Chen; chenxbok@126.com

Received 12 November 2018; Revised 8 March 2019; Accepted 23 June 2019; Published 14 July 2019

Academic Editor: P. Davide Cozzoli

CoS/nanocarbon (NC) composites were prepared via a one-pot hydrothermal method and were used as counter electrodes (CEs) in quantum dot-sensitized solar cells (QDSCs). The CoS/nanocarbon (NC) composite thin film CE has been prepared via a one-pot hydrothermal method. Addition of NC to the solution before hydrothermal treatment led to a CoS/NC composite with a good dispersion of conducting NC. The nanoscaled CoS in the composite CE provides abundant catalytic sites, and the carbon particle framework also acts as highly conductive paths for fast charge transport from the counter electrode (highly catalytic CoS active sites) to the photoanode. The optimized CoS/NC composite CE showed a two-order decrease in the charge-transfer resistance, compared to the pure CoS CE. The TiO_2/CdS/CdSe/ZnS-based QDSC using the optimized CoS/NC composite CE shows enhanced photovoltaic performance with a power conversion efficiency of 4.46% and good stability (94.8% retention after 100 h continuous illumination).

1. Introduction

In past years, quantum dot-sensitized solar cells (QDSCs) have attracted significant attention as the next generation of dye-sensitized solar cells (DSSCs). Compared with traditional dyes employed in DSSCs, the strategic advantages of the use of low band gap QDs for light-trapping include widely tunable bandgap, broad spectral ranges, high extinction coefficients, and the expectation to obtain a considerable improvement in power conversion efficiency (PCE) by utilizing multiple exciton generation of QDs [1–3]. For most previously reported high-performance QDSCs, CoS was used as the CE, exhibiting remarkable catalytic activity [1, 4–6]. However, to the best of our knowledge, the pure CoS used as CE material alone is still very limited because of the relatively low electrical conductivity and poor stability for QDSCs. Therefore, many researchers have turned to combine CoS with other conducting materials to overcome the limitation for improving the electrical conductivity and cell performance [4, 5, 7]. Moreover, the specific surface area of the catalyst is another key factor of the counter electrode. The nanocarbon (NC) particles have advantages for photovoltaic applications because of their large surface-to-volume ratio and high electrical conductivity [8, 9], which would result in the effective interaction between the CEs and electrolyte solution and thus lead to an enhancement in charge-transfer efficiency [1, 10]. Accordingly, motivated by the above facts, it is envisioned that CoS composited with NC can provide superior electrocatalytic performance as a CE of a QDSC device by means of their positive synergistic effects.

In this paper, we report a facile one-pot method to prepare a CoS/NC composite CE for high-performance CdS/CdSe QDSCs. We compared the adding amount of NC on the performance of QDSCs with the CoS/NC composite CE under the same conditions. The nanoscaled CoS nanosheets in the CoS/NC composite CE provide an abundance of catalytic sites, and the NC framework acts as an excellent electrical tunnel for improved charge transport from an external circuit to highly catalytic CoS active sites. The optimized CoS/NC-30 composite displayed an enhanced catalytic activity toward polysulfide electrolyte reduction as

a CE, which increased the PCE value to 4.46%, in comparison to either CoS or NC CEs.

2. Experimental Section

2.1. Preparation of CEs. All of the chemical reagents were purchased from Sigma-Aldrich Shanghai Trading Co Ltd. and used without further purification. The CoS/NC composites were prepared by a facile one-pot hydrothermal method. $CoNO_3{\cdot}6H_2O$ (0.2328 g) and CH_4N_2S (0.1218 g) were dissolved in 20 mL of absolute ethanol. A calculated amount of NC powder was suspended in 20 mL ethanediol ultrasonically and then blended with the above solution and 3 mL ethylenediamine under magnetic stirring. The amounts of NC were set at five levels: 10 mg, 20 mg, 30 mg, 40 mg, and 50 mg. The above suspensions were poured into a Teflon-lined autoclave with a capacity of 100 mL and heated at 180°C for 12 h. Then, the product was collected and washed with deionized water and ethanol. The final product was dried at 80°C for 12 h to get the CoS/NC composite. Five different weight ratios of the NC to CoS samples were prepared by the same method and labeled as CoS/NC-10, CoS/NC-20, CoS/NC-30, CoS/NC-40, and CoS/NC-50. The comparison sample (without NC) was also prepared and denoted as CoS. The method used for the formation of the CEs is similar to that described by Yang et al. [11]. To prepare the CEs, 2 g of CoS/NC powder was dispersed into polyvinylidene fluoride (PVDF) with several drops of N-methyl pyrrolidone (NMP) as the solvent and 0.2 g of PVDF as the binder and then milled in a ball mill to form the slurries. And then the slurries were spread on FTO by the doctor blade method to form CE films. The films were air dried at 80°C for 1 h.

2.2. Preparation of Photoanodes and QDSCs. A TiO_2 photoanode was constructed via layer-by-layer assembly of the TiO_2 compact layer, porous TiO_2 layer, and light-scattering layer. In a first step, the TiO_2 compact layer was traditionally prepared by spray pyrolysis at 500°C [12, 13]. Subsequently, an 8 μm thick transparent layer with 20 nm sized anatase TiO_2 particles, followed by another 3 μm thick light-scattering layer combined with 300 nm sized rutile TiO_2 particles for the QD deposition, was screen printed onto the substrate. As-prepared films were dried at 80°C for 0.5 h. After sintering at 450°C for 0.5 h, the film was treated with 30 mM $TiCl_4$ aqueous solution at 70°C for 0.5 h and then further sintered at 500°C for 0.5 h.

2.3. Photoanode Fabrication. The CdS/CdSe/ZnS QDSSCs were deposited onto the TiO_2 photoanodes following the procedure from reference [7]. A CdS seed layer was in situ grown on the TiO_2 SILAR process prior to CdSe deposition. For the preparation of the CdS seed layer, 5 SILAR cycles were conducted, employing $Cd(CH_3COO)_2{\cdot}2H_2O$ aqueous solution (0.1 M) and Na_2S aqueous solution (0.1 M) as the cation and anion source, respectively. CdSe QDs were grown on the surface of the TiO_2/CdS film by a chemical bath deposition (CBD) technique. TiO_2/CdS films were vertically immersed into an aqueous solution (a mixture of 80 mM $CdSO_4{\cdot}8/3H_2O$, 80 mM Na_2SeSO_3, and 90 mM $N(CH_2CO_2H)_3$) at 40°C for 2.5 h. The electrodes were sintered at 300°C in air for 1 h and cooled to room temperature. Finally, after CdSe QD deposition, the films were coated with 2 SILAR cycles of a ZnS passivation layer, by dipping alternatively into 0.1 M $Zn(CH_3COO)_2{\cdot}2H_2O$ ethanol solution and 0.1 M Na_2S methyl alcohol solution for 1 min. At last, the photoanode is labeled as TiO_2/CdS/CdSe/ZnS.

2.4. QDSSC Device Fabrication. The QDSSC device was assembled with a TiO_2/CdS/CdSe/ZnS photoanode, CoS/NC composites or commercial Pt CE, and a polysulfide electrolyte using a Surlyn spacer to maintain a distance of 30 μm between the two facing electrodes. The polysulfide electrolyte was a methanol/water (7:3) solution containing of 1 M Na_2S, 2 M S, and 0.1 M KCl. The active area of the devices was 0.25 cm^2. For stability tests, the assembled QDSSC devices were sealed with an EVA film under hot press.

2.5. Characterizations. The crystal structure was examined by X-ray diffraction (XRD) analysis (X'Pert MPD Pro diffractometer) with Cu Kα radiation operated at 40 kV and 40 mA. The morphologies and elemental compositions of the products were observed by field emission scanning electron microscopy (FE-SEM, Zeiss SUPRA 35VP) equipped with an energy dispersion X-ray spectroscopy (EDS). Transmission electron microscope (TEM) and high-resolution TEM images of the CoS/NC were performed on a JEM-1400 electron microscope. Electrochemical impedance spectroscopy (EIS) was executed on symmetrical cells using an electrochemical workstation (CHI660E, Shanghai Chenhua Device Company, China). The photovoltaic characterization of devices were measured using a solar simulator (Xe Lamp Oriel Sol^3A™ Class AAA Solar Simulator 94023A, USA). The J–V curves were also recorded by a Keithley 2400 source meter.

3. Results and Discussion

3.1. Structures and Morphologies of the Samples. In this section, we use CoS/NC-30 as a representative CoS/NC composite for the study of structures and morphologies. The difference between CoS/NC-10, CoS/NC-20, CoS/NC-30, CoS/NC-40, and CoS/NC-50 was only the different contents of NC. The phase purity and structural properties of as-prepared samples were determined by XRD. Figure 1 shows the XRD patterns of NC, CoS, and representative CoS/NC-30 powders. The diffraction peaks at 26.0° and 44.1° can be assigned to the (002) and (100) planes of the carbon phase (JCPDS no. 26-1080), while the other four major diffraction peaks appeared at $2\theta = 30.7°, 35.3°, 47.0°$, and 54.6° are well indexed to the (100), (101), (102), and (110) planes of the hexagonal phase CoS (JCPDS no. 65-3418), respectively. After being composited with NCs, a small "bulge" near 26.0° for CoS/NC-30 is easily discerned, which reflects the mixed phase structure of its two components confirming the formation of the CoS/NC composite.

The microstructure and morphology of the CoS, NC, and CoS/NC-30 composites are demonstrated by SEM images in Figures 2(a)–2(c). The SEM image shows that the CoS is

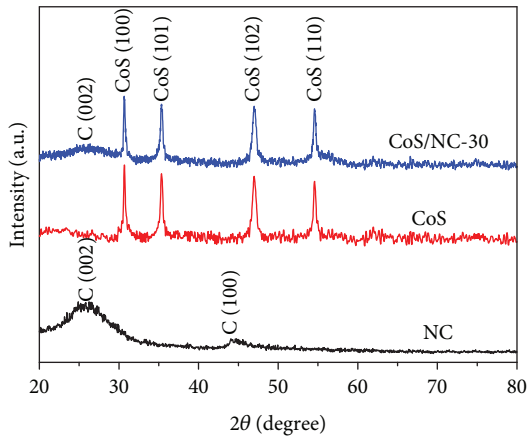

FIGURE 1: XRD spectra of the NC, CoS, and representative CoS/NC-30 powders.

composed of some irregular nanosheets ranged from several tens to hundreds of nanometers in edge size. NC presents as nanoparticles with a size of about 30 nm, as shown by the SEM image (Figure 2(b)) and TEM images (Figures 3 and 3(b)). The CoS nanosheets and NCs can be seen in the CoS/NC-30 composite. Clearly, CoS nanosheets are highly dispersed in the NC matrix. It was clear that the as-prepared CoS/NC-30 composite film had a fine porous structure and there was good electrical contact among the nanoparticles. Moreover, there is sufficient contact between CoS nanosheets and NCs as reflected in the TEM images (Figures 3(c) and 3(d)) of the CoS/NC-30. The microstructure of CoS nanosheets embedded in the NC framework can be clearly seen. This is favorable for electron transfer between CoS nanosheets and NC. The NC framework, together with CoS nanosheets, ensures the large contact surface area of the CoS/NC composite CE, thereby presenting abundant active sites for the reduction of the S_x^{2-} ion [11]. This mesoporous structure will be favorable for improving catalytic activity as compared with the CoS counter electrode due to more active sites being exposed. Similar observations were also reported previously in the cases of $NiCo_2O_4$ or TiN nanoparticles adhering on carbon nanoparticles [14, 15]. Figures 2(d) and 2(e) show the EDS spectrum and EDS mapping images of CoS/NC-30 indicating the homogeneous distribution of Co, S, and C elements. There is a C element exiting in the EDS spectrum analysis, and C is apparently distinguished in the mapping image, indicating that the C materials are highly dispersed around CoS particles.

3.2. Electrochemical Properties. Previous research has already proved that NC can enhance the conductivity of the CE, while NC itself is not a suitable CE material for QDSCs [11, 16]. In order to estimate the effect of the NC content on the performance of CoS/NC composite CEs, five types of the CoS/NC composite with different NC content were successfully fabricated. Pure CoS and NC were also prepared as the reference. These thin film CEs have a similar thickness between 3.2 and 3.7 μm.

Electrochemical impedance spectroscopy (EIS) measurements have been done to study the charge-transfer processes between CEs and the electrolyte. Symmetric dummy cells with two symmetric CEs facing each other were prepared for EIS measurements. Figure 4 shows the Nyquist plots of Pt, pure NC, CoS, CoS/NC-10, CoS/NC-20, CoS/NC-30, CoS/NC-40, and CoS/NC-50 electrodes incorporating with a polysulfide redox electrolyte. One can see that the sheet resistance (R_S) of all CEs can be determined at high frequencies around 100 kHz. For our CEs, the first semicircle in the high-frequency region (between 10 and 100 kHz) corresponds to the solid–solid interface resistance (R_{CT1}) [17]. In the frequency region between 100 Hz and 10 kHz, the impedance was related to the carrier transport at the CE/electrolyte interface including the charge-transfer resistance (R_{CT2}) at the CE/electrolyte interface for I_3^- reduction and the double layer capacitance (constant phase element (CPE)) [18]. The parameters obtained by fitting the impedance spectra with the equivalent circuit shown in Figure 4(a) are summarized in Table 1. R_{CT2} is a pivotal parameter reflecting the catalytic activity of the prepared CEs. The R_{CT2} values of Pt and pure NC CEs are not satisfied (up to several hundred Ω cm^2), indicating that their catalytic activity was unacceptably low in the polysulfide electrolyte. The R_{CT2} value decreases in the order of Pt ($375.69\,\Omega\,cm^2$) > pure NC ($233.28\,\Omega\,cm^2$) > CoS ($115.16\,\Omega\,cm^2$) > CoS/NC − 50 ($69.34\,\Omega\,cm^2$) > CoS/NC − 40 ($67.52\,\Omega\,cm^2$) > CoS/NC − 10 ($18.56\,\Omega\,cm^2$) > CoS/NC − 20 ($16.18\,\Omega\,cm^2$) > CoS/NC − 30 ($14.47\,\Omega\,cm^2$). CoS/NC-30 CE achieves the lowest R_{CT2} value of 14.47 Ω cm^2, indicating that NC strongly enhances the charge-transfer ability of the CoS/NC composite-based CEs, though optimal amount of NC in CoS/NC composite CEs can enhance the conductivity properties of CE, and extremely excessive amounts will decrease the amount of effective catalytic sites of CoS nanosheets in the CoS/NC composite CE and therefore lead to a higher value of R_{CT2} (up to 69.34 Ω cm^2) for CoS/NC-50 CE. The similar finding was reported in the literature [11]. The largest differences between the CoS/NC composite-based CEs and pure CoS CE are probably related to the strength of bonding between CoS nanosheets or NCs within the film, which can be indicated from their microstructural properties presented above. As for the CoS/NC-based CEs, the CoS nanosheets have compact linkage with the NC particles, creating a valid framework to support the CoS nanosheets. The NC framework serves as the good electron transport tunnels and thus notably reduces the total internal resistance of the CoS/NC composite CEs, which ensures the efficient exploitation of highly catalytic CoS nanosheets. In the case of pure CoS CE, the poor connections between the loose stacked CoS nanosheets would create a bottleneck for the reflux electrons (the electrons flowing from the external circuit to the CE). This suggests that catalytic active sites on CoS nanosheets may not be efficiently utilized, thus leading to a higher overall R_{CT2} value.

3.3. Photovoltaic Characteristics. Figure 5 shows the photocurrent–voltage (J–V) curves for QDSCs based on various CEs measured under AM1.5 sunlight illumination

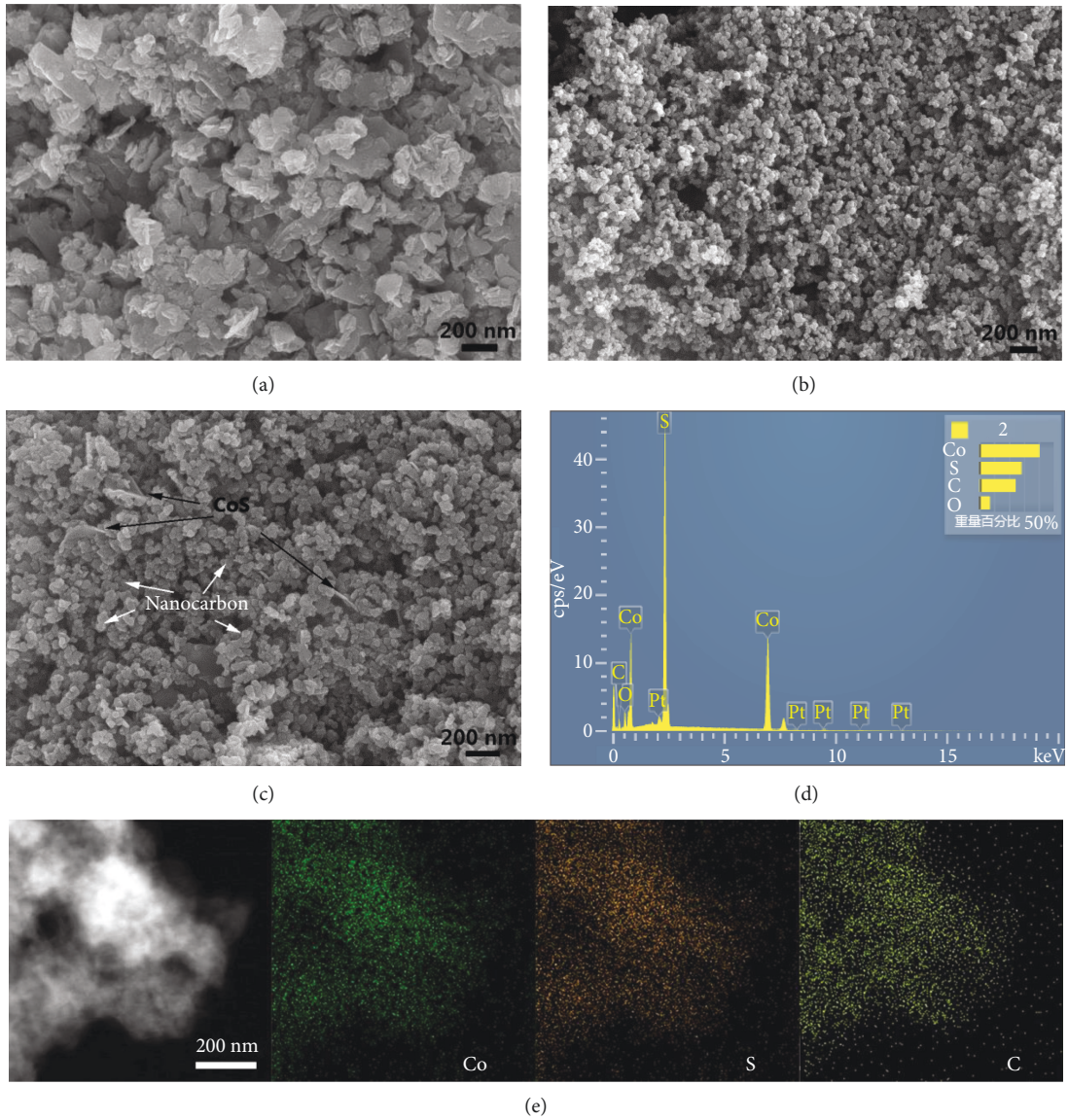

FIGURE 2: SEM images of (a) CoS nanosheets, (b) NC powder, and (c) CoS/NC-30 composite. (d) HAADF-STEM image and the corresponding EDS mapping images of CoS/NC-30. (e) EDS spectrum of the CoS/NC-30 composite.

(100 mW cm^{-2}), and the photovoltaic parameters are summarized in Table 2. The QDSC using CoS/NC-30 CE shows optimal PCE ($\eta = 4.46\%$), with improvement in the short-current density ($J_{SC} = 14.68$ mA cm^{-2}) and open-circuit voltage ($V_{OC} = 0.549$ V) compared to that of the pure CoS. In contrast, the QDSCs based on pure CoS CE exhibit a J_{SC} of 13.46 mA cm^{-2}, a FF of 54%, and a PCE of 3.12%, while NC by itself was not an appropriate CE material, showing relatively poor performance (PCE = 2.26%). The Pt CE-based QDSC shows a much lower PCE (1.36%), owing to the poor catalytic activity of these CE materials when immersed in polysulfide electrolyte. The other samples CoS/NC-10, CoS/NC-20, CoS/NC-30, CoS/NC-40, and CoS/NC-50 have also been investigated and are expected to get improved performances over pure CoS. Consistent with the EIS analysis, the devices with these five CEs (CoS/NC-10, CoS/NC-20, CoS/NC-30, CoS/NC-40, and CoS/NC-50) exhibit a certain increase in J_{SC} over pure CoS-based QDSCs, indicating the enhancement of charge transfer and a lowering of the overall internal resistance of the device by the NC. The negative effect of excessive amount of NC can be clearly seen by the detectable decrease of FF in QDSCs based on CoS/NC-50.

The long-term stability has been considered as one of the most crucial issues that limit the practical application of QDSCs. The CoS catalyst compositions together with the PVDF binder and conductive NC provide good physical contact between CE active materials and the FTO film, thereby resulting in the observed increase in the long-range stability of the CoS/NC CE. The stability of sealed QDSSCs with

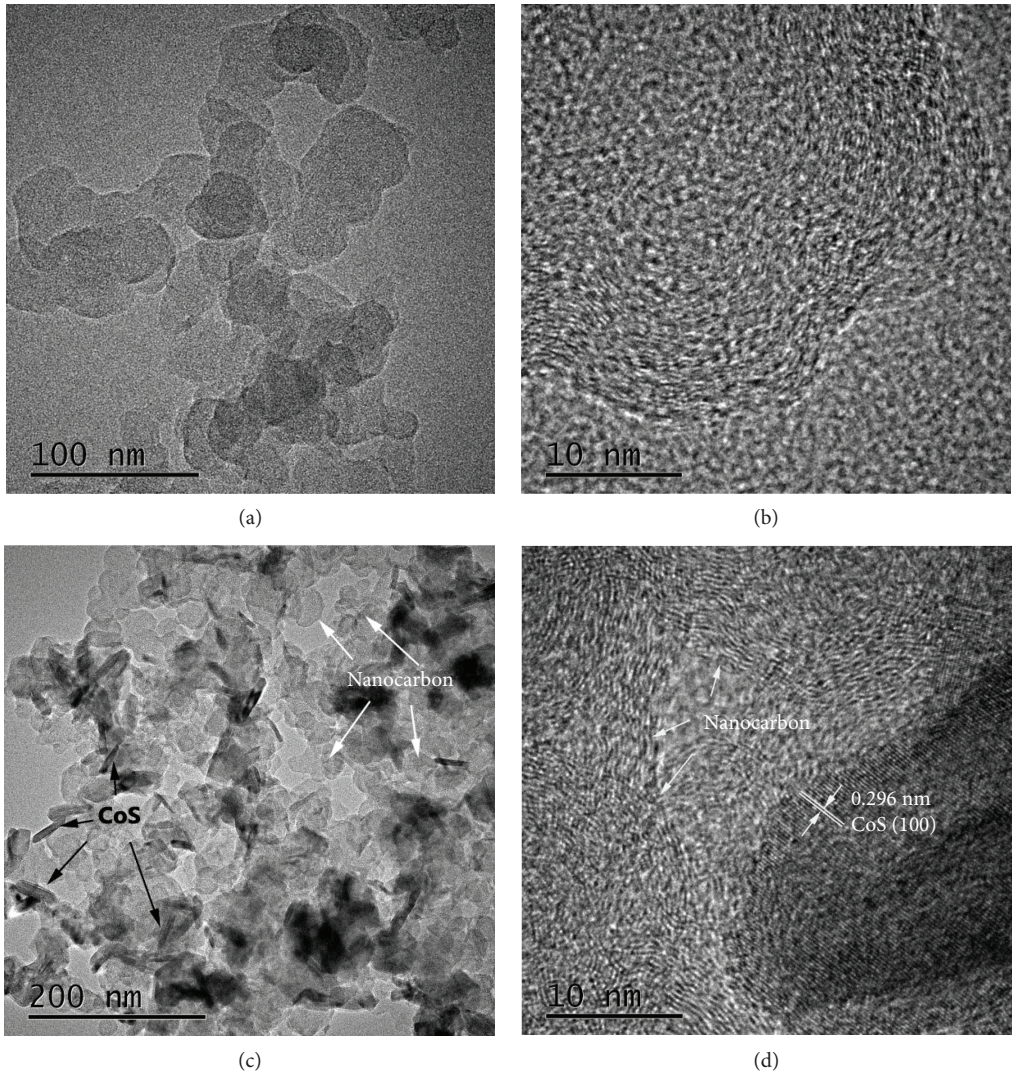

Figure 3: TEM (a) and HRTEM (b) images of the NCs; (c) TEM and (d) HRTEM images of the CoS/NC-30 composite.

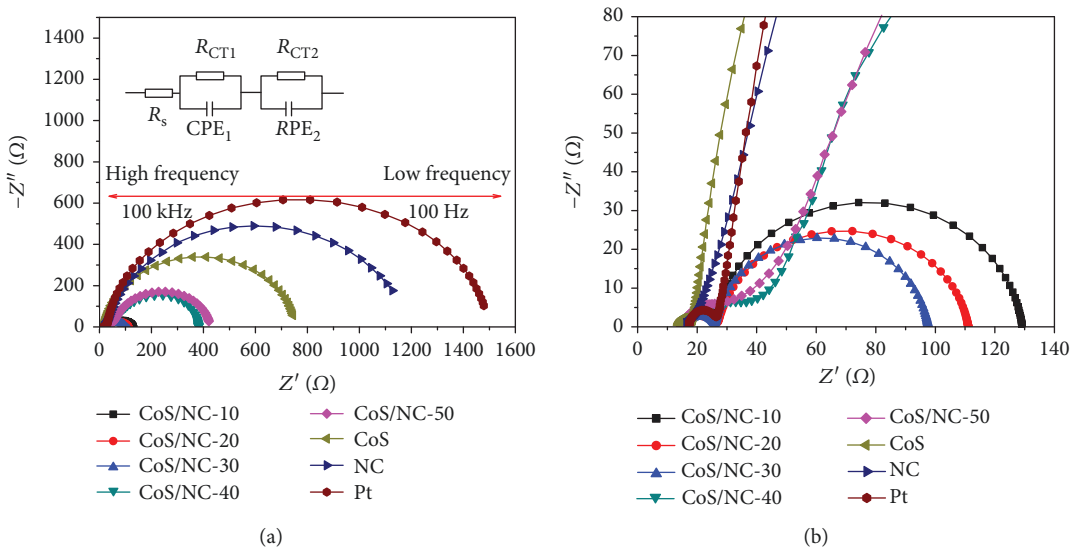

Figure 4: (a) Nyquist plots of symmetric dummy cells with various CoS-based CEs, Pt CE, and pure NC CE measured at zero bias potential; inset: the equivalent circuit for fitting EIS plots. (b) Magnified plots of (a).

Table 1: Fitted impedance values of various CEs.

CE samples	CoS/NC-10	CoS/NC-20	CoS/NC-30	CoS/NC-40	CoS/NC-50	CoS	Pure NC	Pt
R_s (Ω)	9.84	9.68	9.96	9.97	9.94	10.63	9.92	10.86
R_{CT1} (Ω cm^2)	0.91	0.46	0.31	4.21	3.15	19.35	0.34	0.72
R_{CT2} (Ω cm^2)	18.56	16.18	14.47	67.52	69.34	115.16	233.28	375.69

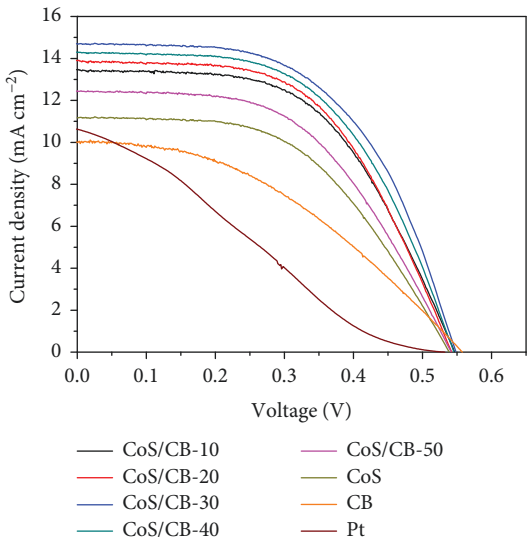

Figure 5: J–V properties of QDSCs with different CEs under a constant illumination intensity of AM1.5 100 mW/cm^2.

Table 2: Output photovoltaic characteristics of the QDSCs with different CEs.

CEs	V_{oc} (V)	J_{sc} (mA cm^{-2})	FF	PCE (%)
CoS/NC-10	0.547	13.46	0.54	4.01
CoS/NC-20	0.542	13.89	0.54	4.11
CoS/NC-30	0.549	14.68	0.55	4.46
CoS/NC-40	0.546	14.29	0.55	4.27
CoS/NC-50	0.541	12.45	0.52	3.51
CoS	0.539	11.17	0.52	3.12
NC	0.557	9.99	0.41	2.26
Pt	0.533	10.63	0.24	1.36

CoS and CoS/NC-30 composite CEs was investigated under continuous illumination for 100 h, as shown in Figure 6. The PCE of CoS/NC-30 and CoS-based QDSSCs showed a stable increase in the first few hours, which can be partially attributed to a capillary effect of the nanochannel structure of TiO_2, and improved ionic transport due to heating of the electrolyte [19]. The PCE of QDSSCs based on the CoS/NC-30 and CoS CEs retained 94.8% and 83.2% of its initial value for continuous illumination for 100 h. This indicated that the CoS/NC-30 CE is highly stable working

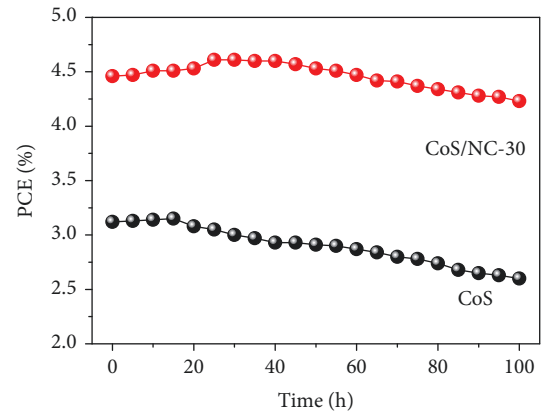

Figure 6: Comparison of power conversion efficiency of QDSSCs based on CoS/NC-30 and CoS CEs under continuous illumination with simulated solar light (air mass 1.5 G, 1 sun condition) for 100 h.

in the QDSC. Moreover, the existence of NC in the CoS/NC composite can serve as the framework to hold the CoS and act as a "nanobridge" to facilitate the electron transport and collection and ultimately improve the efficiency of QDSC. As shown in Table 3, the photovoltaic parameters obtained from our sample are comparable with those in the previous reports. The purpose of Table 3 is to serve as a relative comparison between the present QDSC and those QDSCs containing sulfide CEs. Compared to the previous reports, the PCE of the CoS/NC-30-based QDSC reported in this manuscript achieves the outstanding value.

4. Conclusions

In summary, CoS/NC composite CEs with high electrocatalysis and stability have been synthesized using a low-cost and simple one-pot hydrothermal method. The CoS/NC composite catalyst with appropriate amount of NC can result in better enhancement of both electrical conductivity and catalytic activity. The solar cell obtained with the optimized CoS/NC-30-based CE reaches a high PCE of up to 4.46%. The CoS/NC-30-based CE achieves the lowest R_{CT1} value of 0.31 Ω cm^2, which is two orders of magnitude lower than that of pure CoS. The present study shows that addition of NC directly into the solution prior to hydrothermal treatment prevents the increase in electronic conductivity of CoS. In the meantime, the stability test of sealed QDSC with CoS/NC-30 CE for 100 h proves that the CoS/NC-30 CE is highly stable working in the QDSC. In conclusion,

Table 3: Result comparisons of present photovoltaic parameters with other reports of similar counter electrodes.

CEs	QD	Active area (cm^2)	V_{oc} (V)	J_{sc} (mA cm^{-2})	FF	PCE (%)	References
CoS/NC-30	CdS/CdSe/ZnS	0.25	0.549	14.68	0.55	4.46	This work
CoS/GO sheet	CdS/CdSe	0.16	0.45	14.3	0.44	2.9	[4]
CoS NRA@GP	CdS/CdSe	/	0.60	12.6	0.36	2.70	[6]
CNT/CoS	CdS/CdSe/ZnS	/	0.609	16.14	0.589	5.78	[7]
Cu_2S/C	CdS/CdSe	/	0.47	11.87	0.59	3.37	[16]
Cu_2S/carbon	CdS/CdSe	0.12	0.59	13.69	0.48	3.87	[20]
Cu_2S@RGO	CdS/ZnS	0.16	0.57	8.67	0.47	2.36	[21]
CoS	CdS/CdSe	0.2	0.52	11.2	0.32	1.9	[22]
NiS	CdS/CdSe/ZnS	0.27	0.597	11.67	0.466	3.25	[23]
CuS	CdS/CdSe/ZnS	/	0.57	11.54	0.529	3.48	[24]

the high-quality CoS/NC composite presented a promising application prospect in QDSCs.

Data Availability

The data used to support the findings of this study are included within the article.

Conflicts of Interest

The authors declare that they have no conflicts of interest.

Acknowledgments

This work was supported by the Key Applied Basic Research Program of Yunnan Province (Grant No. 2017FA024), the Program for Innovative Research Team (in Science and Technology) in University of Yunnan Province, the Natural Science Foundation of the Jiangsu Higher Education Institutions of China (Grant No. 17KJB140029), and the QingLan Project of Jiangsu Province.

Supplementary Materials

Figure S1 was added to provide the evidence that the cell realization procedure allows the realization of CdS/CdSe/ZnS quantum dots. The measured lattice spacing in Figure S1 is in accordance with the d-spacing of TiO_2, CdS, ZnS, and CdSe. *(Supplementary Materials)*

References

[1] S. Peng, T. Zhang, L. Li et al., "3D Cu-doped CoS porous nanosheet films as superior counterelectrodes for quantum dot-sensitized solar cells," *Nano Energy*, vol. 16, pp. 163–172, 2015.

[2] X. Lan, S. Masala, and E. H. Sargent, "Charge-extraction strategies for colloidal quantum dot photovoltaics," *Nature Materials*, vol. 13, no. 3, pp. 233–240, 2014.

[3] Y. Bai, C. Han, X. Chen et al., "Boosting the efficiency of quantum dot sensitized solar cells up to 7.11% through simultaneous engineering of photocathode and photoanode," *Nano Energy*, vol. 13, pp. 609–619, 2015.

[4] H. Hu, J. Ding, J. Qian, Y. Li, L. Bai, and N. Yuan, "Layered CoS/graphene nanocomposite as high catalytic counter electrodes for quantum dot-sensitized solar cells," *Materials Letters*, vol. 114, pp. 7–10, 2014.

[5] S. S. Khalili, H. Dehghani, and M. Afrooz, "Composite films of metal doped CoS/carbon allotropes; efficient electrocatalyst counter electrodes for high performance quantum dot-sensitized solar cells," *Journal of Colloid and Interface Science*, vol. 493, pp. 32–41, 2017.

[6] M. Que, W. Guo, X. Zhang et al., "Flexible quantum dot-sensitized solar cells employing CoS nanorod arrays/graphite paper as effective counter electrodes," *Journal of Materials Chemistry A*, vol. 2, no. 33, pp. 13661–13666, 2014.

[7] C. V. V. Muralee Gopi, S. Ravi, S. S. Rao, A. Eswar Reddy, and H. J. Kim, "Carbon nanotube/metal-sulfide composite flexible electrodes for high-performance quantum dot-sensitized solar cells and supercapacitors," *Scientific Reports*, vol. 7, no. 1, article 46519, 2017.

[8] D. S. Su, S. Perathoner, and G. Centi, "Catalysis on nano-carbon materials: Going where to?," *Catalysis Today*, vol. 186, no. 1, pp. 1–6, 2012.

[9] Z. Czech, A. Kowalczyk, R. Pełech et al., "Using of carbon nanotubes and nano carbon black for electrical conductivity adjustment of pressure-sensitive adhesives," *International Journal of Adhesion and Adhesives*, vol. 36, pp. 20–24, 2012.

[10] S. Han, D. Wu, S. Li, F. Zhang, and X. Feng, "Porous graphene materials for advanced electrochemical energy storage and conversion devices," *Advanced Materials*, vol. 26, no. 6, pp. 849–864, 2014.

[11] Y. Yang, L. Zhu, H. Sun et al., "Composite counter electrode based on nanoparticulate PbS and carbon black: towards quantum dot-sensitized solar cells with both high efficiency and stability," *ACS Applied Materials & Interfaces*, vol. 4, no. 11, pp. 6162–6168, 2012.

[12] J. Shi, J. Liang, S. Peng, W. Xu, J. Pei, and J. Chen, "Synthesis, characterization and electrochemical properties of a compact titanium dioxide layer," *Solid State Sciences*, vol. 11, no. 2, pp. 433–438, 2009.

[13] S. Peng, L. Tian, J. Liang, S. G. Mhaisalkar, and S. Ramakrishna, "Polypyrrole nanorod networks/carbon nanoparticles composite counter electrodes for high-efficiency dye-sensitized solar cells," *ACS Applied Materials & Interfaces*, vol. 4, no. 1, pp. 397–404, 2012.

[14] Y. Wang, N. Fu, P. Ma et al., "Facile synthesis of $NiCo_2O_4$/-carbon black composite as counter electrode for dye-sensitized solar cells," *Applied Surface Science*, vol. 419, pp. 670–677, 2017.

[15] G. R. Li, F. Wang, J. Song, F. Y. Xiong, and X. P. Gao, "TiN-conductive carbon black composite as counter electrode for dye-sensitized solar cells," *Electrochimica Acta*, vol. 65, pp. 216–220, 2012.

[16] M. Deng, S. Huang, Q. Zhang et al., "Screen-printed Cu_2S-based counter electrode for quantum-dot-sensitized solar cell," *Chemistry Letters*, vol. 39, no. 11, pp. 1168–1170, 2010.

[17] T. N. Murakami, S. Ito, Q. Wang et al., "Highly efficient dye-sensitized solar cells based on carbon black counter electrodes," *Journal of the Electrochemical Society*, vol. 153, no. 12, pp. A2255–A2261, 2006.

[18] A. Hauch and A. Georg, "Diffusion in the electrolyte and charge-transfer reaction at the platinum electrode in dye-sensitized solar cells," *Electrochimica Acta*, vol. 46, no. 22, pp. 3457–3466, 2001.

[19] K. Zhao, H. Yu, H. Zhang, and X. Zhong, "Electroplating cuprous sulfide counter electrode for high-efficiency long-term stability quantum dot sensitized solar cells," *Journal of Physical Chemistry C*, vol. 118, no. 11, pp. 5683–5690, 2014.

[20] D. M. Li, L. Y. Cheng, Y. D. Zhang et al., "Development of Cu2S/carbon composite electrode for CdS/CdSe quantum dot sensitized solar cell modules," *Solar Energy Materials and Solar Cells*, vol. 120, pp. 454–461, 2013.

[21] A. Hessein, F. Wang, H. Masai, K. Matsuda, and A. A. El-Moneim, "One-step fabrication of copper sulfide nanoparticles decorated on graphene sheets as highly stable and efficient counter electrode for CdS-sensitized solar cells," *Japanese Journal of Applied Physics*, vol. 55, no. 11, article 112301, 2016.

[22] N. Balis, V. Dracopoulos, K. Bourikas, and P. Lianos, "Quantum dot sensitized solar cells based on an optimized combination of ZnS, CdS and CdSe with CoS and CuS counter electrodes," *Electrochimica Acta*, vol. 91, pp. 246–252, 2013.

[23] Y.-S. Lee, C. V. V. M. Gopi, M. Venkata-Haritha, S. S. Rao, and H. J. Kim, "Electrochemical growth of NiS nanoparticle thin film as counter electrode for quantum dot-sensitized solar cells," *Journal of Photochemistry and Photobiology A: Chemistry*, vol. 332, pp. 200–207, 2017.

[24] I. K. Durga, S. S. Rao, A. E. Reddy, C. V. V. M. Gopi, and H. J. Kim, "Achieving copper sulfide leaf like nanostructure electrode for high performance supercapacitor and quantum-dot sensitized solar cells," *Applied Surface Science*, vol. 435, pp. 666–675, 2018.